

HYDROCARBON REACTION IN CORONA DISCHARGE¹

M. Kawahata, J.C. Fraser, and J.A. Coffman

Advanced Technology Laboratories
General Electric Company
Schenectady, New York

-
1. This paper includes part of an investigation on "the coal hydrogenation by electric corona discharge", under the contract with the Office of Coal Research, Department of Interior.
-

INTRODUCTION

When an electric field (a-c in this paper) is applied to the series combination of a gaseous gap and a dielectric solid, the gas will break down and conduct at an applied voltage much lower than that required to break down the solid. The current increases rapidly with an increase in voltage. The dielectric barrier acts as a series ballast to stabilize the corona discharge, which appears as a "soft" glow electrical discharge. THIS FORM OF GLOW DISCHARGE AT ATMOSPHERIC PRESSURE IS DEFINED AS "CORONA"² in this paper. The dominant mechanism in corona

-
2. As contrasted with corona, the spark is a form of unstable discharge. Intense ionization along a definite path for a greater part of the electrode distance is a characteristic of spark. The arc is a form of concentrated spark characterized by a high current density at a relatively low voltage.
-

is ionization by electron impact. The free electrons in the gas acquire energy from the applied field, and, colliding with the gas molecules, create additional free electrons and positively charged ions.

Under stable corona electrical discharge in an electric field containing solid dielectric barriers, chemical reactions which only proceed with difficulty by conventional means may take place with reasonable efficiency. The chemical reactions caused by electric discharge are essentially those involving active species, like excited molecules, free radicals and ions, formed by inelastic collisions between accelerated electrons and molecules.

Extensive studies on the chemical reactions of aliphatic hydrocarbons under the electrical discharge were conducted in 1930's by Lind et al (3,4,5). Using methane as a reactant, the

-
3. S.C. Lind and G. Glockler, *J. Am. Chem. Soc.*, **51**, 2811 (1931).
4. S.C. Lind and G.R. Schultze, *ibid.*, **53**, 3355 (1931).
5. S.C. Lind and G.R. Schultze, *Trans. Electrochem. Soc.*, **59**, 165 (1931).
-

formation of free radicals followed by production of molecular hydrogen, and also condensation to higher paraffins was the essential process. Also, the reaction scheme and the reaction products of α -radiolysis were studied. A similarity between reactions in the electric discharge and radiolysis, was postulated by Lind et al (6,7).

-
6. S.C. Lind and G. Glockler, J. Am. Chem. Soc., 52, 4450 (1930).
 7. S.C. Lind and D.C. Bardwell, J. Am. Chem. Soc., 48, 2335 (1926).
-

The radiolysis of methane was investigated more recently in detail, especially to clarify the reaction mechanisms, including the primary and the secondary reaction processes (8,9,10,11,12,13).

-
8. F.W. Lampe, J. Am. Chem. Soc., 79, 1055 (1957).
 9. K. Yang and P.J. Manno, J. Am. Chem. Soc., 81, 3507 (1959).
 10. G.G. Meisels, W.H. Hamill and R.R. Williams, J. Phys. Chem., 60, 790 (1956).
 11. G.G. Meisels, W.H. Hamill and R.R. Williams, J. Phys. Chem., 61, 1456 (1957).
 12. G.J. Mains and A.S. Newton, J. Phys. Chem. 64, 511 (1960).
 13. R.R. Williams, Jr., J. Phys. Chem. 66, 372 (1962).
-

High energy electrons, low energy electrons, γ -ray and x-ray irradiations were employed for decomposition of methane, producing mainly H_2 , C_2H_6 , C_3H_8 , C_4H_{10} , and C_5H_{12} . It was found that the energy yield of the reactions were essentially independent of the radiation source, dosage, and the system pressure (6,7,8,9,10,11,12,13,14). However, because of the extreme complexity of the reaction processes, the mechanism is not yet completely understood.

-
14. S. Shida, Hoshasen Kagaku (Radiation Chemistry), Nikkan-Kogyosha, Tokyo, Japan (1960).
-

Electrical discharge chemistry has not yet studied intensively from the standpoint of chemical engineering except for a few processes (15,16,17). In order to achieve the technical progress in this field,

-
15. T. Rummel, Hochspannungs Entladungsschemie und Ihre Industrielle Anwendung, Munchen, Germany (1951).
 16. G. Glockler, and S.C. Lind, The Electrochemistry of Gases and Other Dielectrics, New York (1939).
 17. Electric Engineering Soc. Ozonizer Committee, Japan, edited by Suzuki Corona-sha, Tokyo, Japan (1960).
-

according to Suzuki et al, it is highly important to investigate the correlation between electric discharge phenomena and the chemical reactions caused by discharge. This includes: (1) clarification of the concentration and energy distribution of ions and electrons in the discharge space, (2) understanding of the probability of excitation and dissociation caused by collisions of molecules with slow electrons, and (3) clarification of the complete energy balance in the discharge reaction.

Recently in this laboratory, studies on hydrocracking of coal, tar, and related hydrocarbons, using an electric discharge system have been undertaken. This work was primarily intended to obtain chemical engineering knowledge of electric discharge chemical processes. As part of the program, decomposition of methane was studied, since this gas is likely to be used as one of the reactants for cracking of hydrocarbons, and further its simple chemical structure is well suited to definitive studies. Similar studies using aliphatic hydrocarbons other than methane were also conducted but they will be reported elsewhere.

EXPERIMENTAL

Apparatus The experimental apparatus is shown schematically in Figure 1-a. Methane was fed to the reactor with a definite flow rate determined by a rotameter. Then, the product gases were passed through a sampling bottle and a dry testmeter. The reactors employed in this investigation were essentially concentric electric discharge tube similar to ozonizers. The dimensions and the materials of the electrodes were varied, as summarized in Table 1. In Table 1, the discharge space, V , in cc., total surface area, S , in cm^2 , and the logarithmic average of the outside and inside electrode area, A , in cm^2 are listed together. On one side of the quartz electrode, a silver or tin oxide coating served as the electrically conductive surface. In order to determine the reactor temperature, thermistors were attached to the outside electrode and a thermometer was placed in the inside electrode. The electrical system is shown schematically in Figure 1-b.

The corona generating equipment used in these experiments consists of a high voltage, high frequency power supply, with associated instrumentation to control and measure the corona power generated. The output of a 10,000 cycle, 30 KW, inductor-alternator is fed to the primary of a 50 KV, high voltage transformer and, in turn, to a tuned circuit, to a corona cell, and to the high voltage instrumentation. The Basic Power and Instrumentation Circuit is shown on Figure 1-b.

Inductor-alternator output voltage and subsequently, transformer high voltage, are controlled from zero to maximum output by varying the alternator field current.

Since the corona cell itself represents a capacitive load on the inductor-alternator and the transformer, a tuning circuit is provided for power factor correction, so that the high voltage transformer sees only the resistive load represented by the corona power dissipated in the corona cell. This tuning circuit consists of an air-core, foil wound choke and a vacuum-capacitor bank, connected as a parallel resonant circuit across the transformer secondary.

High voltage instrumentation includes a vacuum tube voltmeter operating from a capacitance voltage divider, for reading the peak voltage applied to the corona cell, and a bridge circuit for determining corona power by means of the parallelogram-oscilloscope technique. This technique shows the relationship between the voltage on the cell electrodes at any instant and the charge flow in the circuit up to that instant. Using the area of parallelogram on the oscilloscope, the power input (18) to the reactor was computed.

-
18. The power dissipated in a concentric cylinder corona cell consisting of a gaseous gap in series with solid dielectric barriers can also be calculated from the expression:

$$P = 4fC_b V_g (V_m - V_t)$$

where P is power in watts,
 f is power supply frequency, c.p.s.,
 C_b is capacitance of the dielectric barriers,
 V_g is voltage across gaseous gap at the instant of corona initiation
 V_t is total voltage applied to the corona cell at the instant of corona initiation, and
 V_m is corona cell operating voltage, at some value greater than V_t .

In the above calculation, peak voltage values are used.

Procedures The entire system was first evacuated and methane was introduced to the reactor with a definite flow rate. The voltage applied to the reactor was gradually increased to the gas-space breakdown voltage, at which the electric discharge was initiated. Then, the voltage was adjusted until the parallelogram on the oscilloscope showed the desired discharge wattage. The discharge power was maintained constant during the run. The reaction was usually continued at least for 30 minutes before samples were taken. If there was liquid product in the condenser-I, it was weighed but no attempt was made to analyze it. The gaseous samples were analyzed by mass spectrometer. For reaction at higher temperatures, the methane was heated to the desired temperature in a preheater which was equipped with a temperature controller (West Co.).

EXPERIMENTAL RESULTS

Variation of the Composition with Residence Time The principal reaction products were hydrogen, ethane, propane, butane, pentane and further higher paraffins. In some experimental runs, a small amount of ethylene and propylene was found. In Figure 2 and 3, the variation of the composition with residence time is shown. These two sets of runs were conducted at temperatures between 200 and 230°C under a pressure of 760 mm Hg. The model III reactor was employed, and the current density levels were 0.13 and 0.15 ma./cm.². The current density was computed by using the voltage in the discharge space calculated from the total voltage applied, the discharge wattage and the logarithmic average area of the electrodes A, listed in Table 1. In these figures, the fraction C_2 and C_3 include ethylene and propylene, respectively, and the fraction $+C_4$ includes all the higher paraffin homologues.

It was observed that the disappearance of methane and the formation of H_2 , C_2 , C_3 and $+C_4$ were more rapid at the higher current density. In the initial period methane was consumed almost proportionally to time. This fact agrees to the results reported by Lind and Schultze(3) After this period, methane disappeared exponentially with time. It must be noted that in each of three runs having residence time longer than 100 seconds produced a small amount of liquid which was of amber color.

Effect of Temperature on the Initial Rate of Reaction Using the Model II and IV-C reactor, the initial rate of methane disappearance was investigated varying the reaction temperature. The reaction temperature was determined by taking the average of the inside and outside electrode temperatures. In Figure 4, is shown the Arrhenius plot of the initial rate of CH_4 disappearance in atm./sec. Two lines, AA and

BB, could be drawn, and the apparent activation energy of the overall reaction was calculated to be 4 Kcal./mol. The points along the line AA were determined at a current density of 0.095 ma./cm.² and an applied potential of 5 to 5.2 KV. across the discharge space using the model III reactor. The points along the line BB were determined at a current density of 0.15 to 0.17 ma./cm.² using the model IV-C reactor at 4.5 to 5.0 KV. across the discharge space. Both series were made under a pressure of one atmosphere.

Effect of Current Density on the Initial Rate of Reaction In order to correlate the initial rate of methane disappearance with current density, the rate of reaction at 200°C was computed from each rate obtained at various reaction temperatures by using the activation energy of 4 Kcal./mol. (The temperature, 200°C, is just an arbitrary temperature.) The computed rates of reaction are plotted against current density in Figure 5. The rate of reaction increased as the current density increased, following a relationship,

$$-\frac{d(\text{CH}_4)}{dt} = k(j) \quad (1)$$

where the rate is in atm./sec., the current density, j , is in ma./cm.², and k is 0.075 in average.

Electric Discharge in Space Packed with Alundum Grains and Effect of Pressure on the Rate of Reaction The discharge space of the model IV-B reactor was packed with alundum grains having a particle size of 10 x 15 Tyler mesh, to determine any consequent effect on the reaction rate. The total pressure of the system was also varied in two experimental runs. The experimental results are summarized in Table II. For this packed space reactor, the applied voltage required to initiate the discharge was greater and the discharge wattage was smaller than for the reactor without packing. For the packed discharge space reactor, the apparent current density and the apparent reaction rate are listed in Table II. The apparent dielectric constant of the space packed with alundum grains was calculated using Kamiyoshi's correlation (19), and

-
19. K. Kamiyoshi, Science Reports, Res. Inst. Tohoku Univ. Ser.A, 1, 305 (1949), C.A. 45, 5991
-

then the voltage applied to the packed discharge space and the apparent current density were estimated. For better comparison, the reaction rate at 200°C. was calculated for each run and listed in Table II. Since the rate increases with power density, it is seen that the reaction rate is considerably higher in the packed space reactor, and lower at reduced pressure.

Effect of the Uniformity of the Field on the Reaction Rate Using the several reactors having different diameter ratio, D_i/d_o , (the ratio between the inside diameter of the outside-electrode and the outside diameter of the inside-electrode), the possible effect of non-uniformity of the field on the reaction rate was investigated. It must be noted that for the model IV-D and the IV-E reactor, the inside electrode was tungsten rod or wire. (This type of reactor was called a semi-corona reactor by Lind et al.) The catalytic effect of the tungsten surface was assumed insignificant. It was observed that for these two reactors, discharge streamers were formed only around the center electrode, whereas in the other model reactors, numerous fine blueish streamers extended

from the inside electrode to the outside electrode resulting in formation of blue glow in all the discharge space.

The experimental results are listed in Table III. In the second experimental run, the IV-D reactor failed by arcing between the electrodes. Similarly, the experiment using the IV-E reactor was hindered by the formation of several hot spots on the tungsten electrode which resulted in arc-over between the electrodes. For better comparison, the reaction rates at 200°C were calculated using an activation energy of 4 Kcal/mol. and they are also listed in Table III. Taking into account the difference in current density, the reaction rate seemed lower in the reactor having larger D_i/d_o .

DISCUSSIONS

Based on studies of the radiolysis of methane, the following four steps may be considered to be of primary importance in the decomposition of methane by electric discharge:

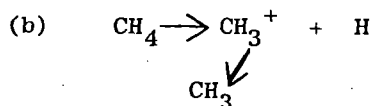
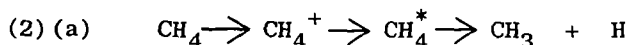
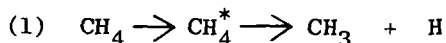
- (1) Formation of excited molecules by inelastic collisions with electrons having sufficiently high energy, and subsequent decomposition to free radicals and/or atoms.
- (2) Ionization of molecules and subsequent neutralization of ions, resulting in formation of free radicals.
- (3) Ion-molecule reactions (20), forming larger ions, and subsequent neutralization leading to formation of neutral molecules and free radicals.

20. F.W. Lampe, J.L. Franklin, and F.H. Field, Kinetics of the Reactions of Ions with Molecules, in Progress in Reaction Kinetics, Vol. I, 67, Pergamon Press, New York, (1961).

-
- (4) Combination of free radicals or reaction of free radicals with molecules (21).

21. E.W.R. Steacie, Atomic and Free Radical Reactions, Reinhold Publishing Corp., New York (1954).

Thus, for example, the formation of ethane could be explained by the following steps:



If more than one kind of electron-reactant reaction is involved simultaneously, integral must be replaced by the sum of the integrals. In this investigation, the initial rate of methane consumption was found to be proportional to the current density when other factors are kept constant. Except for the initial time period, proportionality of the rate to the partial pressure of the reactant was also found as shown in Figure 2 and 3 which show the variation of methane concentration exponential to time. Taking into account the difference in current density, it is seen that proportionality between the rate and the pressure somewhat deviates for the packed bed reactor shown in Table II. This may be due to an uncertainty in estimation of the apparent dielectric constant of the alundum grains packed space and, therefore, in current density. However, as a first approximation, equation (2) seems to apply to this work.

Before corona is initiated the total applied voltage is distributed across the cell components inversely as their capacitance. Then, the voltage and gradients in a concentric cylinder reactor, just before the start of corona, can be expressed by the following expression:

$$E = \frac{V}{r k_g} \left[\frac{1}{\ln \left[\frac{(D_o/D_i)(d_o/d_i)}{k_b} \right] + \frac{\ln(D_i/d_o)}{k_g}} \right] \quad (3)$$

where, E is the field at any point in radius, r ,
 V is the total applied voltage,
 k_g and k_b are the dielectric constant for gas and barrier,
 respectively,
 D_o and D_i are the outside and inside diameter of the outside
 electrode, and
 d_o and d_i are the outside and inside diameter of the inside
 electrode.

After corona is initiated, the total applied voltage is distributed across the cell components directly as their impedance. However, this does not alter the equation (3) greatly.

Since,

$$\left(\frac{D_o}{D_i} \right) \left(\frac{d_o}{d_i} \right) \sim 1.0, \quad (4)$$

the equation (3) becomes

$$E \sim \frac{(1)}{(r)} \left[\frac{V}{\ln(D_i/d_o)} \right] \quad (5)$$

The drift velocity, W , and the integral term in equation (2) are a function of E/p , where p is the pressure. Thus, the overall rate of reaction becomes the integral of the equation (2) with respect to radial distance. Increasing the diameter ratio, D_i/d_o , appeared to cause a decrease in the overall rate of reaction. Since the exact expressions of $Q(V)$, $f(V)$, and W are not available, the analysis of the data is qualitative. Nevertheless, for the reactor having larger D_i/d_o , apparently a possible faster reaction rate in the strong field near the center electrode was overbalanced by the slower rate in the weak field portion of the reactor.

The rate of reaction was significantly increased, when the reactor discharge space was packed with alundum grains. This increase in the

rate cannot be explained clearly. Higher field in the packed space, surface reaction effects, if any, or higher concentration of high energy electrons in a smoothly diffused discharge formed in a packed space could be the reasons.

The energy yield of the process is shown in Figure 6, where energy introduced per unit mol. is plotted against methane consumption in per cent. The calculated reaction rates at 200°C were used for the plot. The slope, that is, the average energy spent per mol. of methane consumed was 1980 Kcal/mol. at 200°C for the initial period. The best result was obtained for the alundum grain packed reactor at 267°C. and the energy yields were 740, 1090, 3000, and 9000 Kcal per mol. of CH₄ disappearance, and H₂, C₂H₆ and +C₃ formation, respectively. The corresponding G values were 3.1 (-CH₄), 2.1 (H₂), 0.77 (C₂H₆) and 0.26 (+C₃). These values are about one-half of the values obtained by radiolysis (6,7,8,9,10,11,12,13,14).

ACKNOWLEDGEMENTS

The authors wish to thank T. H. Phoenix and G.A. Techy for their assistance in this experimental work, G. P. Schacher for mass spectrographic analysis, and N. R. Dibelius and C. D. Doyle for valuable discussions.

TABLE I
DIMENSIONS OF THE REACTORS

Reactor	Outside Electrode			Inside Electrode		
	Material	O.D. D_o mm	I.D. D_i mm	Material	O.D. d_o mm	I.D. d_i mm
II	quartz	19.0	17.0	quartz	11.0	9.0
III	quartz	45.7	42.4	quartz	35.3	32.0
IV-A	quartz	45.7	42.4	quartz	35.3	32.0
IV-B	quartz	20.0	18.0	quartz	12.0	10.0
IV-C	quartz	12.1	10.0	quartz	4.0	3.0
IV-D	quartz	9.5	7.3	tungsten	1.05	---
IV-E	quartz	8.5	8.3	tungsten	0.33	---

Reactor	Electrode Length L mm.	Discharge Space V cc.	Total Area S cm. ²	Average Cylindrical Area A cm. ²	Diameter Ratio D_i/d_o
II	78	10.3	71.7	34.0	1.5
III	400	168.0	975.0	488.0	1.2
IV-A	200	84.0	488.0	244.0	1.2
IV-B	200	29.0	188.0	93.0	1.5
IV-C	200	13.2	87.5	41.0	2.5
IV-D	200	8.2	52.5	20.4	7.0
IV-E	200	6.2	41.5	12.7	19.0

TABLE II

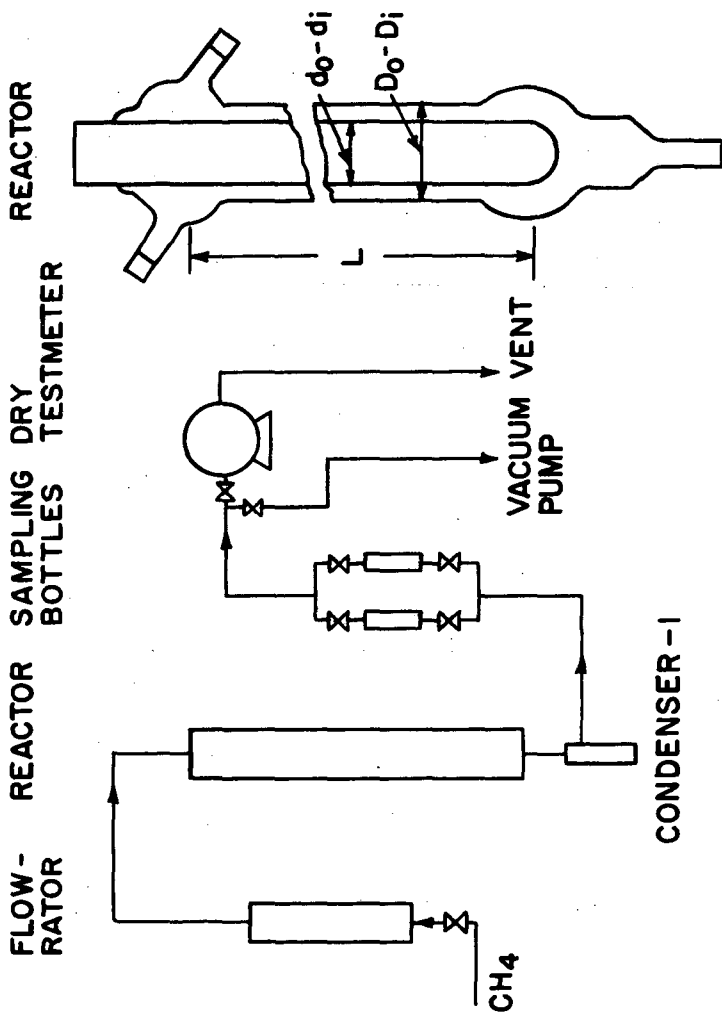
EFFECT OF THE REACTOR SPACE PACKED WITH ALUNDUM
GRAINS AND OF PRESSURES ON THE REACTION RATE
(IV-B REACTOR)

Exp. No.	Reactor Packing	Pressure mm.Hg	Temp. °C.	KV kv. g	Current Density, j_2 ma./cm. ²	Rate (atm./sec.) $\times 10^2$	Computed Rate at 200°C (atm./sec.) $\times 10^2$
9-24-3-1	no	760	280	5.1	0.17	2.7	1.5
9-24-3-2	Al ₂ O ₃ grains	760	267	5.8	0.083	2.1	1.3
9-25-3-1	Al ₂ O ₃ grains	238	225	4.1	0.13	1.6	1.3
9-25-3-2	Al ₂ O ₃ grains	280	325	4.0	0.12	2.2	0.87

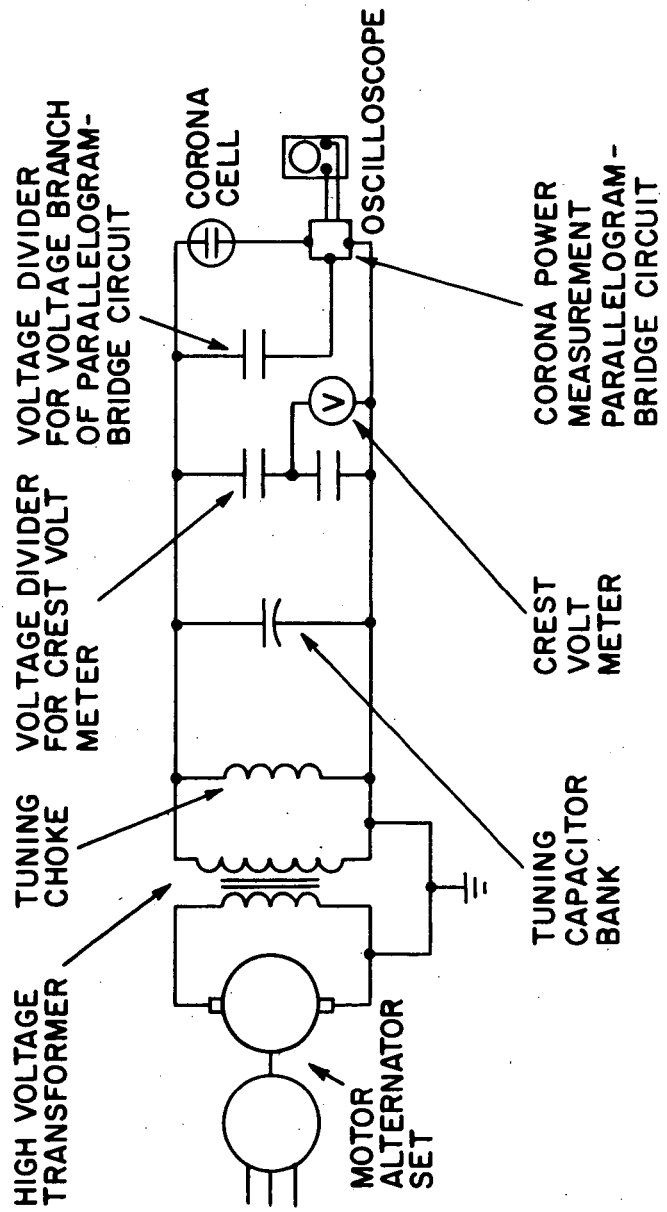
TABLE III

EFFECT OF UNIFORMITY OF THE FIELD ON THE REACTION RATE

Exp. No.	Reactor	D_1/d_0	Temp. °C.	KV kv. g	Current Density, j_2 ma./cm. ²	Rate (atm./sec.) $\times 10^2$	Computed Rate at 200°C (atm./sec.) $\times 10^2$
9-24-3-1	IV-B	1.5	280	5.1	0.17	2.7	1.5
9-9-3	IV-C	2.5	215	5.0	0.15	1.1	1.0
9-11-31-1	IV-C	2.5	318	4.5	0.18	2.7	1.2
9-6-3	IV-D	7.0	217	4.8	0.32	1.9	1.7
9-16-3-1	IV-E	19.0	80	3.9	0.33	0.33	1.4
9-16-3-2	IV-E	19.0	110	4.4	0.32	0.48	1.3

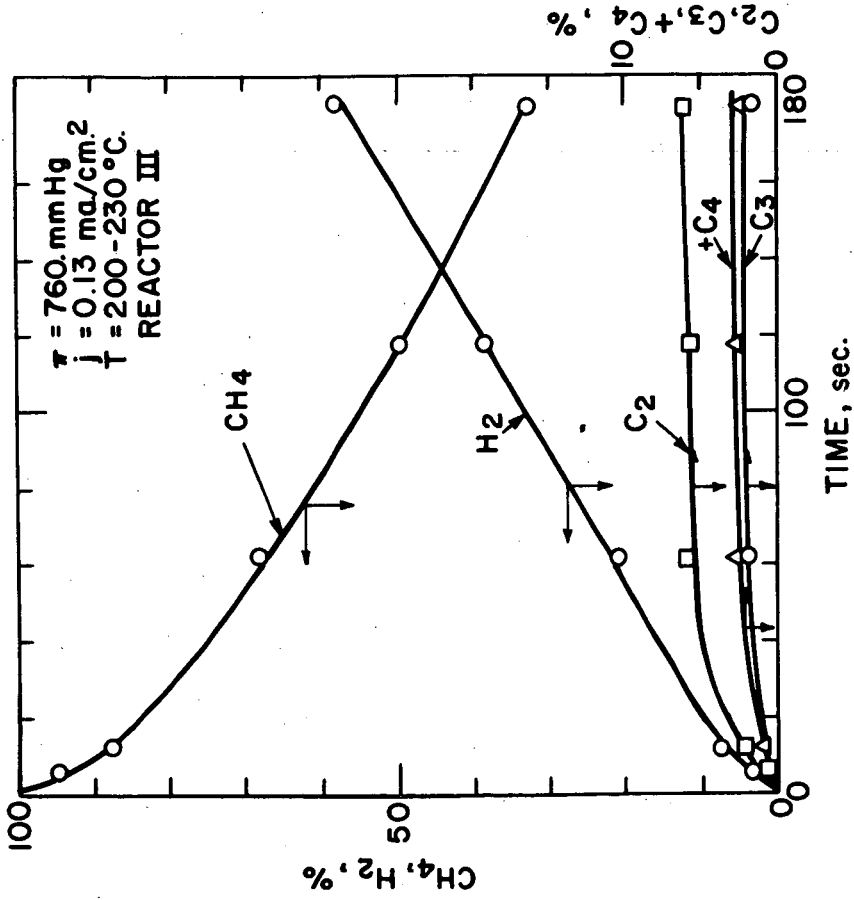


FLOW DIAGRAM OF THE APPARATUS
AND THE REACTOR
FIGURE 1-a

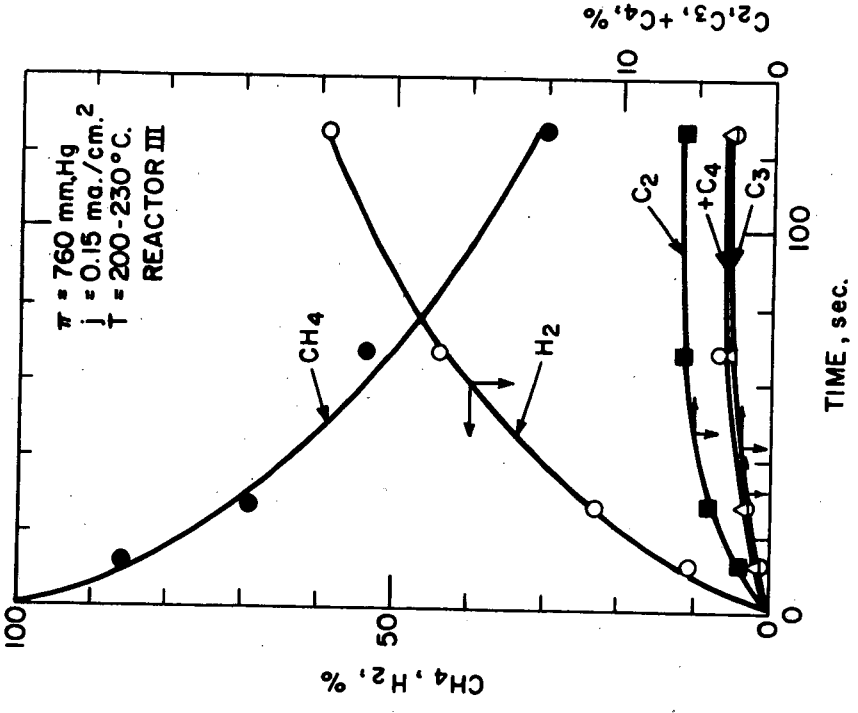


BASIC POWER AND INSTRUMENTATION CIRCUIT

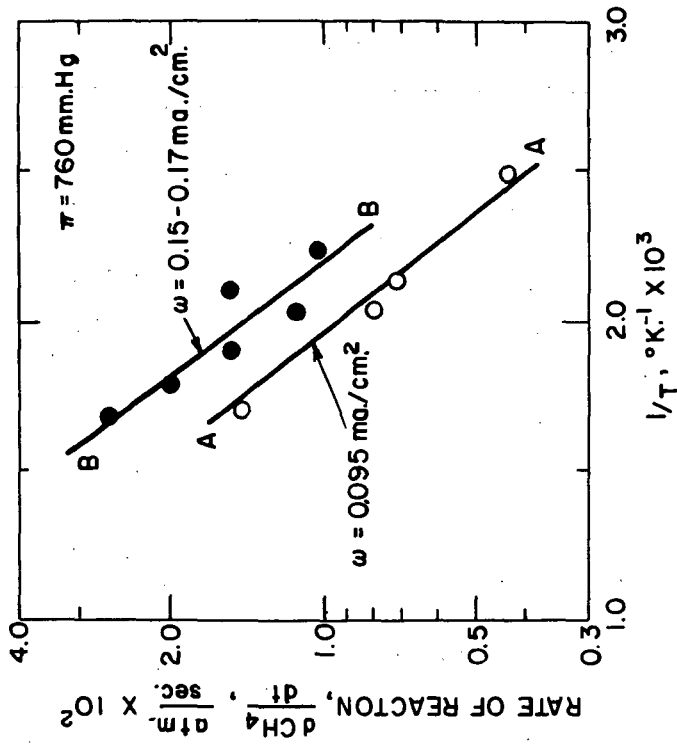
FIGURE 1-b



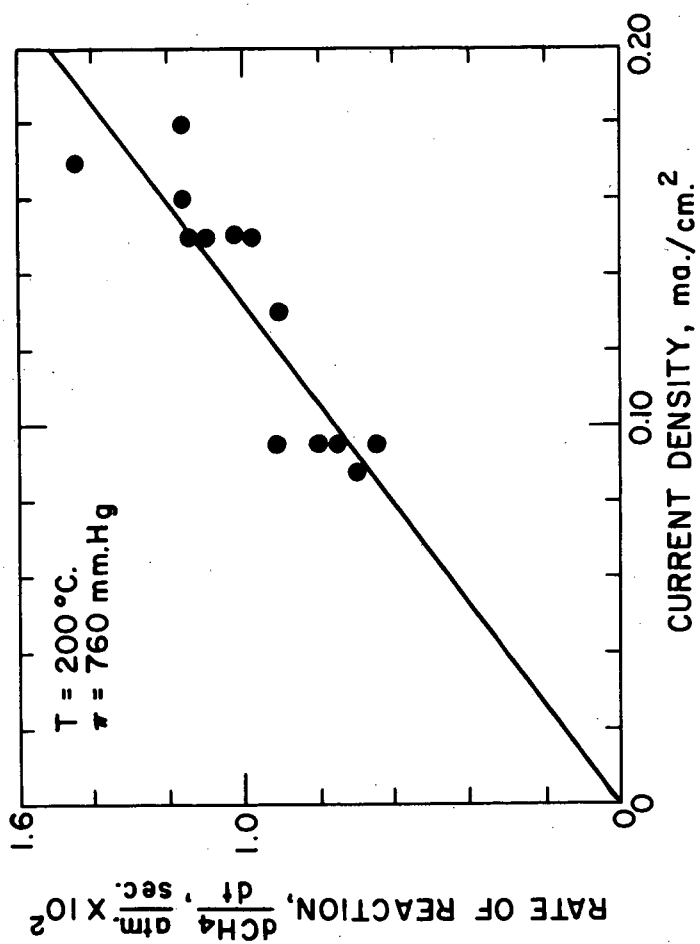
VARIATION OF COMPOSITION OF PRODUCT GASES WITH TIME
 FIGURE 2



VARIATION OF COMPOSITION OF PRODUCT GASES WITH TIME
FIGURE 3

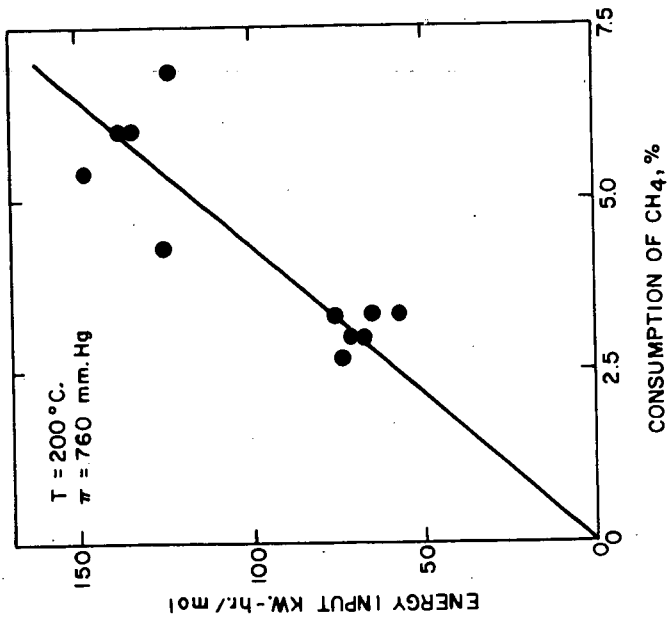


ARRHENIUS PLOT OF THE OVERALL
 RATE OF REACTION
 FIGURE 4



VARIATION OF RATE OF REACTION
WITH CURRENT DENSITY

FIGURE 5



VARIATION OF CH₄ CONSUMPTION
WITH ENERGY INPUT
FIGURE 6